Synchronization, clustering, and weak chimeras in a densely coupled transcription-based oscillator model for split circadian rhythms [REE]

Special Collection: Chimera states: from theory and experiments to technology and living systems

Jorge Luis Ocampo-Espindola ⁽¹⁾; K. L. Nikhil ⁽¹⁾; Jr-Shin Li ⁽¹⁾; Erik D. Herzog ⁽¹⁾; István Z. Kiss ¹



Chaos 33, 083105 (2023)

https://doi.org/10.1063/5.0156135





Citation

CrossMark





Synchronization, clustering, and weak chimeras in a densely coupled transcription-based oscillator model for split circadian rhythms

Cite as: Chaos 33, 083105 (2023); doi: 10.1063/5.0156135

Submitted: 26 April 2023 · Accepted: 8 July 2023 ·

Published Online: 3 August 2023



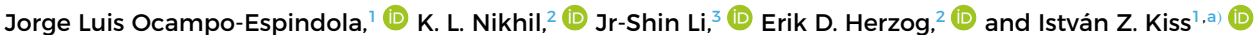














AFFILIATIONS

- Department of Chemistry, Saint Louis University, 3501 Laclede Ave., St. Louis, Missouri 63103, USA
- ²Department of Biology, Washington University in St. Louis, One Brookings Drive, St. Louis, Missouri 63130-4899, USA
- Department of Electrical and Systems Engineering, Washington University in St Louis, 1 Brookings Drive, St. Louis, Missouri 63130, USA

Note: This paper is part of the Focus Issue on Chimera states: from theory and experiments to technology and living systems. a) Author to whom correspondence should be addressed: istvan.kiss@slu.edu

ABSTRACT

The synchronization dynamics for the circadian gene expression in the suprachiasmatic nucleus is investigated using a transcriptional circadian clock gene oscillator model. With global coupling in constant dark (DD) conditions, the model exhibits a one-cluster phase synchronized state, in dim light (dim LL), bistability between one- and two-cluster states and in bright LL, a two-cluster state. The two-cluster phase synchronized state, where some oscillator pairs synchronize in-phase, and some anti-phase, can explain the splitting of the circadian clock, i.e., generation of two bouts of daily activities with certain species, e.g., with hamsters. The one- and two-cluster states can be reached by transferring the animal from DD or bright LL to dim LL, i.e., the circadian synchrony has a memory effect. The stability of the one- and two-cluster states was interpreted analytically by extracting phase models from the ordinary differential equation models. In a modular network with two strongly coupled oscillator populations with weak intragroup coupling, with appropriate initial conditions, one group is synchronized to the one-cluster state and the other group to the two-cluster state, resulting in a weak-chimera state. Computational modeling suggests that the daily rhythms in sleep-wake depend on light intensity acting on bilateral networks of suprachiasmatic nucleus (SCN) oscillators. Addition of a network heterogeneity (coupling between the left and right SCN) allowed the system to exhibit chimera states. The simulations can guide experiments in the circadian rhythm research to explore the effect of light intensity on the complexities of circadian desynchronization.

Published under an exclusive license by AIP Publishing. https://doi.org/10.1063/5.0156135

Circadian rhythms control the sleep-wake cycles of animals by synchronization of the nearly 24h period oscillations of individual clock cells in the brain region called the suprachiasmatic nucleus (SCN). Under normal conditions, the cells synchronize and generate daily bouts of activities. Some animals, for example, hamsters, under constant light conditions, can show two bouts of daily activities (split circadian rhythms) separated by nearly 12 h, similar to biphasic sleep. This phenomenon was explained by the left- and right-brain SCN cells oscillating 12 h apart. We developed a biomolecular model for the SCN to show that light can induce such behavior by a synchronization pattern in which two groups of oscillators form. In each group, the oscillators are synchronized in-phase, but the two groups are anti-phase synchronized. When two such populations are considered, for

example, representing the SCN in the left and right brain, a chimera state was observed, when one group synchronizes in onecluster and the other group in a two-cluster (split) state. The model predictions can be used to better understand the properties of the circadian clock, in particular, under varying conditions such as the transition from constant dark to bright/dim light and back.

I. INTRODUCTION

Synchronization of oscillatory processes is an important dynamical phenomenon with relevance to many physical, chemical, and biological processes.1 With chemical oscillators, early studies used stirred tank reactors (CSTRs)2-6 and showed different synchronization patterns, e.g., in-phase, anti-phase, and out-ofphase entrainment in small networks. Large networks of oscillatory units can be built, for example, with Belousov-Zhabotinsky (BZ) microdroplets,^{7,8} beads,^{9,10} microwell arrays,¹¹ and nanodroplets¹² or with electrochemical oscillators. 13 Globally coupled electrochemical oscillators showed a variety of synchrony patterns with various levels of coherence, including full synchrony¹⁴ and other stable¹⁵ and intermittent¹⁶ cluster states. In a globally coupled network, bistability was found between one- and two-cluster states with electrochemical oscillators 15 where the frequency synchronized oscillators had identical phases (one cluster) or form two clusters, which are often nearly anti-phase.

In many biological systems, an optimal level of synchronization is required.¹⁷ Chimeras are types of patterns that can realize a state with an intermediate level of synchrony with coexisting domains of coherence and incoherence in networks of identical oscillators. 18,19 Many traditional chimeras considered a continuum limit of infinitely many oscillators. 20,21 The concept of "weak chimera"22,23 provides a rigorous definition of chimera-like states in networks with the finite number of oscillators yet capture essential features of the original chimeras:20 Weak chimeras exhibit localized frequency synchrony in networks of identical oscillators.²² Such states were discovered with modular networks of phase models with higher-order phase interaction functions^{22–24} and later confirmed with synchronization engineering techniques with electrochemical oscillators, where a network of two pairs of oscillators was locked in-phase and anti-phase configurations, respectively, with different frequencies.²⁵ Similarly, in a modular network of electrochemical oscillators, two populations with weak cross-coupling synchronized in one- and two-cluster states with different frequencies to yield a weak-chimera state.2

The circadian clock presents an important example where a synchronized network of oscillatory units with a period close to 24 h, i.e., the network of the circadian cells in the suprachiasmatic nucleus (SCN), and regulates a large variety of behavioral and physiological functions.²⁷⁻³⁰ The oscillatory gene expression in an SCN cell can be described with ordinary differential equation (ODE) models. 27,31-35 The SCN cells, as heterogeneous autonomous oscillators, 36 are typically synchronized to a one-cluster state 37 and thus the animal exhibits approximately one bout of daily activity separated by a sleep phase. However, splitting of the daily activity into two components was observed with hamsters transferred to constant light conditions.³⁸⁻⁴¹ Seasonal changes in activity patterns can include two bouts of daily activity (e.g., around dawn and dusk on long days) as an adaptation to resource availability.³⁸ On a biomolecular level, splitting was found to be related to the leftand the right-brain SCN gene expressions cycling in 12 circadian hours apart.⁴⁰ This splitting of the circadian activity can be modeled with coupled nonlinear oscillators where circadian cells synchronize in anti-phase configurations. 38,42-46 Multicellular, biomolecular models are capable of describing the synchronization of the SCN cells to a fully (or partially) synchronized one-cluster state.^{47,48} The constant light-induced two-cluster (splitting) state challenged our current understanding of the circadian clock because many possible dynamical mechanisms can explain similar cluster states. For example, phenomenological models predicted that splitting could occur when the constant light switches the coupling sign between the oscillators from positive to negative or through delays/inhibitions. 43,44,46 A biomolecular model 49 was developed that showed that such assumptions may not be needed because when the maximum transcription rate of the essential clock gene was increased by light intensity, the circadian properties of the individual clock cells change, and the coupling between two circadian cells changes from phase attractive to phase repulsive. Therefore, in a modular network with very strong coupling in each of the two populations (where the phase repulsive coupling is counterbalanced by amplitude coupling resulting in a one-cluster state), and weak coupling between the populations, light intensity increase induces a switch from in- to anti-phase collective synchronization between the populations.45

In this paper, a network model with transcriptional clock gene oscillators is investigated to clarify the mechanism of the splitting in the form of synchronized (or partially synchronized) two-cluster states to seek new dynamical splitting mechanisms and to explore the possibility of the existence of weak-chimera states in a model SCN. First, numerical simulations were performed in a globally coupled SCN model at various light intensities to identify the parameter region where stable one- and two-cluster states could exist. The goal was to show that, in a realistic biomolecular SCN model, two-cluster states emerge with increase of light intensity even with a symmetrical network and identical oscillator properties. The stability of the oneand the two-cluster states are interpreted with a theoretical analysis⁵⁰ using phase models extracted from the ODE models using both phase sensitivity function^{15,51,52} and data-based⁵³⁻⁵⁷ approaches. The capability of the two types of phase models to predict the stability of the clusters is compared. The presence of the weak-chimera state is confirmed in a modular model where two populations of SCN cells (representing the two nuclei of the SCN) are coupled weakly. Finally, the relevance of the stability of the one- and the two-cluster states and the observed chimera states to the properties of the circadian clock are discussed.

II. MATERIALS AND METHODS

A. SCN model

1. Model equations: Single circadian clock and coupling

We considered a simplified model for the kinetics of a clock gene for each circadian cell in the SCN.33,58 The model consists of three variables, concentrations of the core circadian clock mRNA (M) and the corresponding clock protein in the cytosol (P_c) and the nucleus (P_{nuc}). The ODE model is constructed to consider the salient kinetic features of the transcription process: the inhibition of the maximum transcription rate by $\bar{P_{\mathrm{nuc}}}$, the Michaelis–Menten type degradation of M and P_c , and the diffusion of the proteins between the cytosol and the nucleus,5

$$\tau_k \frac{dM_k}{dt} = \nu_{s,k} \frac{K_I^4}{K_I^4 + P_{max}^4} - \nu_m \frac{M_k}{K_m + M_k},\tag{1}$$

$$\tau_{k} \frac{dM_{k}}{dt} = \nu_{s,k} \frac{K_{I}^{4}}{K_{I}^{4} + P_{\text{nuc},k}^{4}} - \nu_{m} \frac{M_{k}}{K_{m} + M_{k}},$$
(1)
$$\tau_{k} \frac{dP_{c,k}}{dt} = k_{s} M_{k} - \nu_{d} \frac{P_{c,k}}{K_{d} + P_{c,k}} - k_{1} P_{c,k} + k_{2} P_{\text{nuc},k},$$
(2)

$$\tau_k \frac{dP_{\text{nuc},k}}{dt} = k_1 P_{c,k} - k_2 P_{\text{nuc},k},\tag{3}$$

where $k=1,\ldots,N$ denotes the cell index in a population of N=200 cells. The parameters were selected to produce circadian oscillations: 49 $v_m=0.421$ nM/h, $K_I=1.0$ nM, $K_m=0.5$ nM, $k_s=0.417$ 1/h, $v_d=1.167$ nM/h, $K_d=0.13$ nM, $k_1=0.417$ nM/h, $k_2=0.5$ nM/h. The inherent heterogeneities of the individual cells are modeled by choosing the values of τ_k (time scale parameter) from a Gaussian random distribution of mean 1.000 and standard deviation 1.0×10^{-3} . In the case of identical oscillators, $\tau_k=1$.

A key model parameter is the maximum transcription rate, $v_{s,k}$. Following previous studies, we assumed that light intensity increases the maximum transcription rate $(v_{s,k})$ in each cell. $^{33,47-49,59}$ In addition, the coupling between the cells is also mediated by $v_{s,k}$. Based on the signaling mechanism of the coupling, 48 it is assumed that the mRNA level of cell j (M_j) promotes the release of the vasoactive intestinal protein (VIP); the VIP enters the intercellular medium and binds to the VPAC2 protein, which regulates the mRNA expression (maximum rate) of cell k through Ca^{2+} and CREB. In other words, when M_j increases, the maximum transcription rate of cell k also increases. Altogether, the effect of light and coupling can be modeled by Ref. 49,

$$\nu_{s,k} = \nu_0 + L + \alpha (M_i - M_k), \tag{4}$$

where $v_0=0.73$ nM/h is the base maximum transcription rate, L is the light intensity, and α is the coupling strength. We note that this basic model was not built to reproduce all the dynamical features of the circadian clock. Instead, it captures the salient dynamical features such as self-sustained oscillations, response to light by phase shifts, and coupling induced synchronization. And Many other features are not included, for example, the presence of the multiple core genes of the complex dynamics of light transduction to the SCN. We have considered some features that enabled us to obtain splitting yet retain some of the known biomolecular properties of the gene expressions.

2. Model equations: Networks

The circadian cells can be coupled assuming an all-to-all global coupling scheme, in which each cell is affected by all other cells, i.e.,

$$v_{s,k} = v_0 + L + \alpha \sum_{j=1}^{N} (M_j - M_k).$$
 (5)

The nature of global coupling is certainly a simplification of the complex network coupling of the SCN cells; however, it reflects the presence of a dense network resulting in robust synchrony and allows the use of the theory of globally coupled oscillators for predictions of the synchronization states. Efforts to infer the functional connections within the SCN have revealed network topologies including all-to-all and small world depending on the experimental conditions and functional network being mapped. To better reflect the network organization of SCN cells, we also investigated the behavior of a modular network, when the N=200 cells are divided in two populations. The cells for $k=1,\ldots,100$ were assigned to population 1 and $k=101,\ldots,200$ to population 2. In

each population, the coupling strength is α as in Eq. (5), however, the coupling between the populations is somewhat weaker, $\alpha\epsilon$, where ϵ is the cross coupling parameter $(0 \le \epsilon \le 1)$,

$$v_{s,k} = v_0 + L + \alpha \sum_{j=1}^{100} (M_j - M_k)$$

$$+ \alpha \epsilon \sum_{j=101}^{200} (M_j - M_k) \quad k = 1, 2, \dots 100,$$
(6)

$$\nu_{s,k} = \nu_0 + L + \alpha \epsilon \sum_{j=1}^{100} (M_j - M_k) + \alpha \sum_{j=101}^{200} (M_j - M_k) \quad k = 101, 102, \dots 200.$$
 (7)

B. Phase definition and measure of cluster synchronization

The oscillatory behavior of the time series $M_k(t)$ was characterized by its frequency (or period) and phase. We used the peakfinding technique to reconstruct the phase of each oscillation. The peak mRNA expression $M_k(t)$ for each cell was identified as t_k^l , where l is the peak number. The phase can be determined by assuming that two consecutive peaks are separated by 2π and at other times, the phases are linearly interpolated, i.e.,

$$\theta_k(t) = \frac{t - t_k^{l-1}}{t_k^l - t_k^{l-1}} 2\pi.$$
 (8)

The phases were unwrapped to increase continuously with time. The frequency was obtained from the slope of the phase vs time plot and the period as the inverse of the frequency.

The extent of cluster synchronization was calculated using the phases with the generalized order parameters⁶³ according to

$$r_n(t) = \frac{1}{N} \sum_{k=1}^{N} e^{ni\theta_k(t)},$$
 (9)

where i is the complex unit and n=1 or 2. R_1 and R_2 are the average over time of the absolute value of $r_1(t)$ and $r_2(t)$, respectively. When $R_1 \approx R_2 \approx 0$, the system is desynchronized, while $R_1 \approx R_2 \approx 1$, the system is synchronized in a one-cluster configuration. If $R_1 \approx 0$ but $R_2 \approx 1$, the system is synchronized in a two-cluster configuration.

C. Actogram generation from the SCN model

To illustrate the dynamical behavior observed in the SCN cells, we assumed that the changes of the concentration of the M variable (\dot{M}) resulted in locomotor activity (W), which we plotted as an actogram. We considered the animal to be active when the single population mean < M > decreases and inactive when < M > increases. When $< \dot{M} > \le 0$ then the activity was scaled with steep sigmoid function $W(t) = \tanh(-25 < \dot{M}(t) >)$, and zero otherwise. Therefore, W can be considered to be proportional to the normalized wheel running activity in the range of 0 to 1. W can be visualized

using an actogram where W is plotted as the height of the shaded area as a function of time for each day. For the modular network, W was calculated as the sum of the two population activities. This definition is similar to other studies that generated actograms. 44,49

III. RESULTS AND DISCUSSION

A. Uncoupled cells: Free-running period distributions at different light intensities

First, we considered the behavior of the oscillatory circadian gene expressions for the uncoupled populations, i.e., $\alpha = 0$. The free-running periods of the individual oscillations of $M_k(t)$ were determined under three different light intensities: constant darkness (DD, L = 0.00), dim light (LL, L = 0.27), and bright light (LL, L = 0.32). For constant darkness and light, we use the common notations DD and LL, respectively, widely used in circadian biology. 65 As shown in Fig. 1(a), in DD conditions (L = 0.00), the cells had an average free-running period of 21.97 \pm 0.022 h (mean \pm standard deviation). In dim LL conditions [L = 0.27, see Fig. 1(b)], the mean period increases to 23.57 \pm 0.024 h. Note that, in accordance to previous findings, 49 the oscillations in LL are slower, in this example by about 1.6 h (7%), while the standard deviation is also somewhat wider (by about 9%). This trend also continues for bright LL conditions [L = 0.32, Fig. 1(c)] with a mean free-running period of $23.90 \pm 0.025 \, h$.

B. Simulations of a globally coupled network at different light intensities

We examined the effect of the coupling in a single population SCN model with all-to-all topology. Numerical simulations of a globally coupled network were performed from random initial conditions at a fixed coupling strength ($\alpha=1.8\times10^{-4}$); the results are shown for DD (row a), dim LL (rows b and c), and bright LL (row d) conditions in Fig. 2. At each condition, a numerical simulation was performed from a random initial condition, and we determined the snapshot of the phases for each cell, the time series of M(t), and the actogram.

At DD $[L=0.00, \, {\rm Fig.} \,\, 2(a)]$, the globally coupled population exhibits a fully synchronized behavior: the gene expressions time series nearly overlap, and the phase differences with respect to the slowest (longest free-running period) oscillator (with index $k=\max P$), $\theta_k-\theta_{maxP}$, are nearly the same. Note that, as expected from phase synchronization theories, 51 the faster oscillators are somewhat ahead of the slowest oscillators in phase difference vs free-running period graph [left panel in Fig. 2(a)]. The simulated actogram for the circadian rhythm [right panel in Fig. 2(a)] shows the expected one bout activity band. The simulations thus confirm that in DD, the SCN synchronizes to a one-cluster state, and the results are consistent with the previous finding that in DD the globally coupled SCN population synchronizes to a nearly one-cluster state.

The behavior of the globally coupled SCN population in dim light conditions (L=0.27), is shown in Fig. 2(b). The time series of $M_k(t)$ shows there is a slight increase in the amplitude of the oscillations with a less sinusoidal waveform compared to DD conditions. In addition, only 36 of the 200 oscillators are synchronized (thick

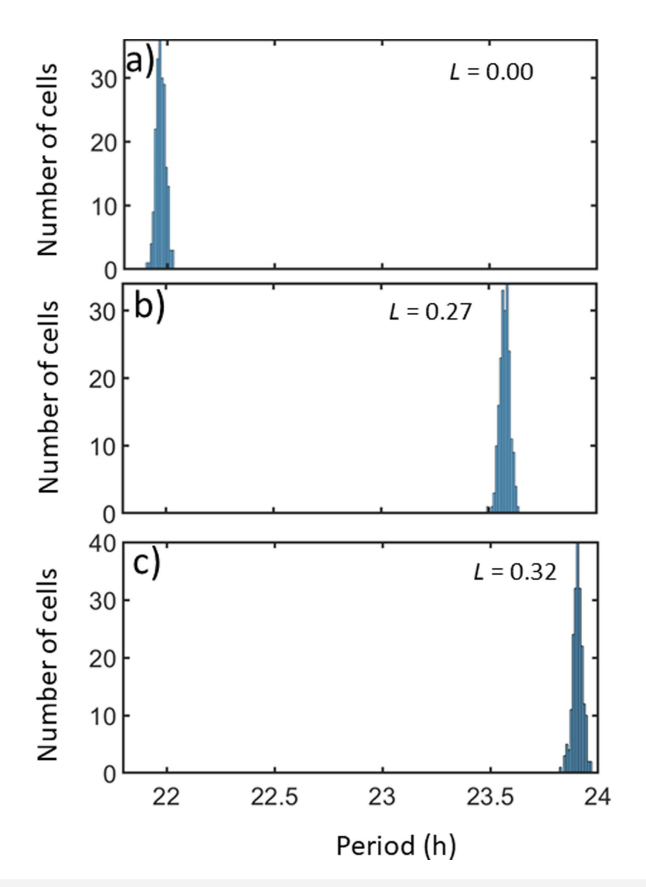


FIG. 1. Histograms of the period distribution of the circadian gene mRNA $(M_k(t))$ oscillations of the uncoupled cells. (a)–(c) Histogram of the period in DD (a, L=0.00), dim LL (b, L=0.27), and bright LL (c, L=0.32).

green curve in the graph), while the rest of the population was desynchronized. The phase-difference graph (left panel) shows that the slow (long free-running period) oscillators are phase locked, and the desynchronized elements are fast (with short free-running period). In the corresponding actogram for the circadian rhythm, there is again one bout of activity due to the synchronized cells in the one-cluster configuration, however, the activity length in a given day is now wider. The results showed that in dim LL, under the given conditions, the population formed a partially synchronized one-cluster

While many random initial conditions in dim LL resulted in a partially synchronized one-cluster state of the SCN, some initial conditions yielded a fundamentally different synchronization state. The $M_k(t)$ time series shows two groups of anti-phase synchronized oscillations [shown as thick red and green curves in Fig. 2(c)] along with some desynchronized elements. As in the previous case, the elements with a long free-running period were phase-locked but now with two phases separated by about π . The actogram features two bouts of activities, characteristic of a split circadian rhythm. Under these conditions, the system exhibits a partially synchronized

Chaos ARTICLE pubs.aip.org/aip/cha

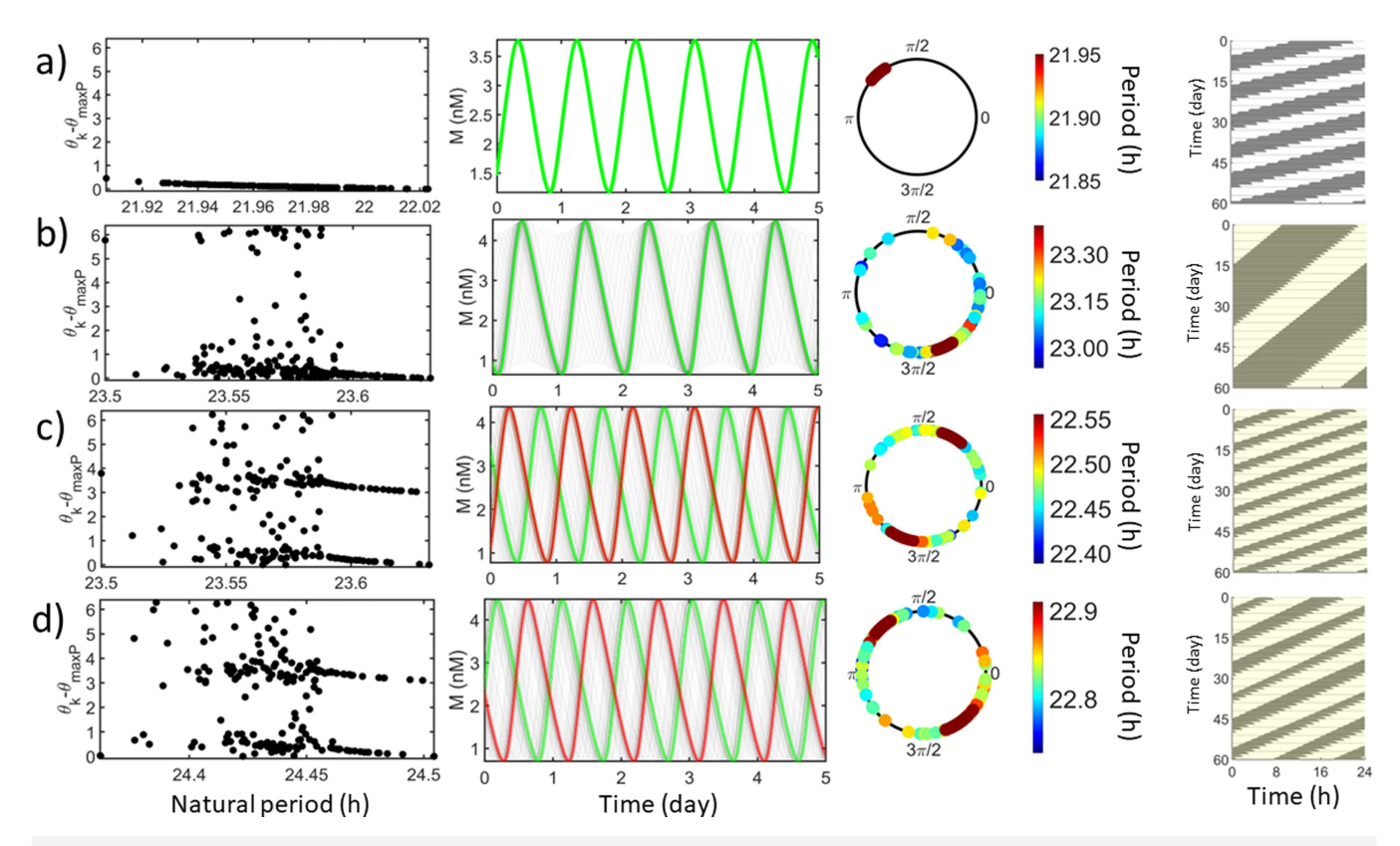


FIG. 2. Synchronization states of a single population SCN model in DD (row a), dim LL (rows b and c), and bright LL (row d) conditions starting from random initial conditions. From left to right: the relative phase of the oscillators (with respect to the slowest oscillator) vs free-running (natural) period, the time series of the mRNA ($M_k(t)$) (thick green or red lines represent frequency synchronized oscillations, with different colors for different phase clusters), a snapshot of the phases, and an actogram. (a) The SCN in DD showed one-cluster synchronization. (b) Partially synchronized one-cluster state in dim LL (L = 0.27). (c) Partially synchronized two-cluster state in dim LL (L = 0.32).

two-cluster state. Thus, in dim LL, there is bistability between the partially synchronized one- and two-cluster states.

When the light intensity was further increased to L=0.32 [bright LL, Fig. 2(d)], the typical behavior of the single population SCN was a partially synchronized two-cluster state. The $M_k(t)$ time series exhibited two anti-phase synchronized groups with some desynchronized oscillators. Two distinct phase differences were observed at approximately 0 and π for the elements with a long freerunning period, and the actogram showed two bouts activities per day. In bright LL, thus, the SCN exhibits a partially synchronized two-cluster state corresponding to a split circadian rhythm.

Because in dim LL, the final state showed sensitivity to initial conditions, we performed 100 simulations from random initial conditions at each light intensity (DD, dim LL, bright LL) and classified the final state as one- or two-cluster partially synchronized state; the results are shown in Fig. 3. In DD, all initial conditions converged to the one-cluster state. In bright LL, all initial conditions resulted in the two-cluster state. However, in dim LL conditions, 59% of the initial conditions ended up in the one-cluster and 41% in the two-cluster state. These results further confirm that depending on the initial conditions, in dim LL, the SCN exhibits a bistability

between the one-cluster (non-split) and the two-cluster (split) state.

When there is bistability between different synchronization states, it is possible that the splitting of the circadian rhythm depends on the light protocol that had been used before the animal was

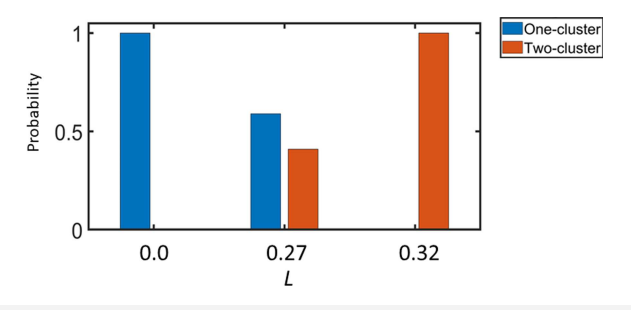


FIG. 3. The distribution of one- and two-cluster synchronized states in the SCN from simulations using one hundred random initial conditions with different light intensities in DD (L = 0.00), dim LL (L = 0.27) and bright LL (L = 0.32).

09 August 2023 16:17:27

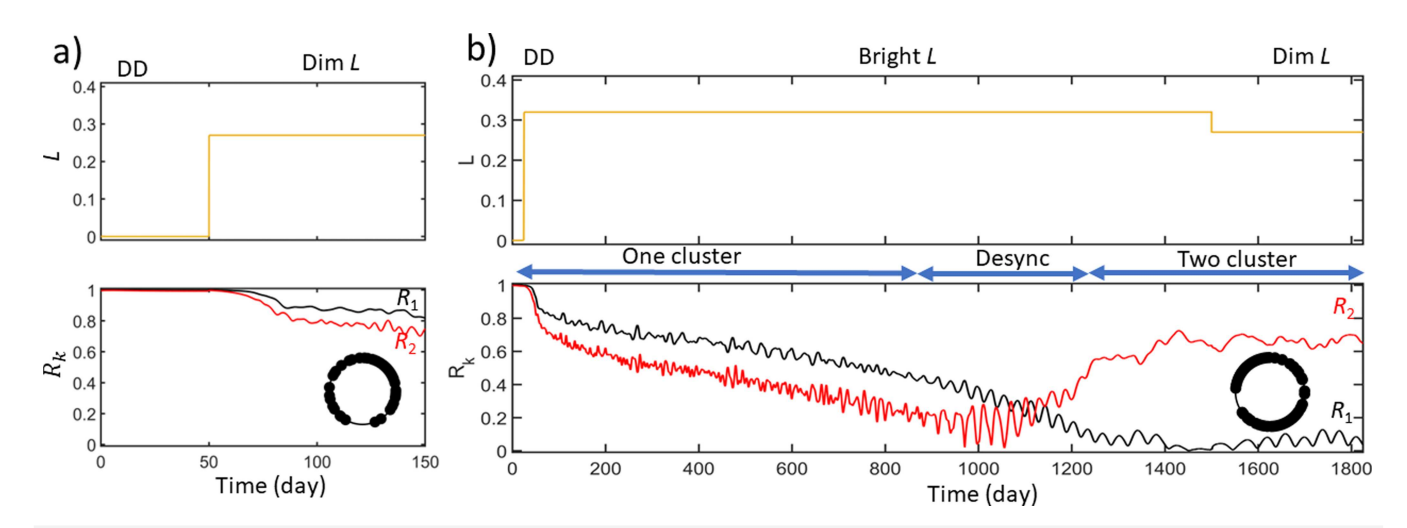


FIG. 4. Simulations of the circadian rhythm by transferring the SCN from DD to dim LL (a) and from DD through bright LL to dim LL (b). Top: light intensity as a function of time. Bottom: The first and second Kuramoto order parameter as a function of time. The inset panels show a snapshot of the phases for each cell in the final state. (a) Transferring the SCN from DD to dim LL, the SCN yielded a one-cluster (non-split) state. (b) Transferring from DD through bright LL to dim LL yields a two-cluster (split) circadian rhythm.

transitioned to dim LL conditions. For example, circadian clocks exhibit prior LD cycle or history dependent changes in rhythms called aftereffects. 66-68 In the following simulations, we demonstrate the bistability by applying DD or bright LL light protocols before dim LL.

Figure 4(a) shows the results when the animal was transferred to dim LL from 50 days in DD. Under DD conditions, the population remained in a complete one-cluster state with synchronization indices $R_1 = 0.99$ and $R_2 = 0.99$. After dim LL at day 50, the order parameters gradually decreased until they stabilized around $R_1 = 0.86$, $R_2 = 0.75$. We, thus, see that when transferring the animal from DD to dim LL results in a non-split circadian rhythm.

Figure 4(b) shows the results when the animal was transferred from DD to bright LL at 50 days ($t = 50 \,\mathrm{d}$) and then from bright LL to dim LL at t = 1500 d. As previously, in DD, a one-cluster state of the SCN was observed. After bright LL at day 50, the order parameters gradually decreased resulting in a partially synchronized state (50 d < t < 880 d), followed by a desynchronization interval $(880 \, d < t < 1250 \, d)$ to the two-cluster state $(1250 \, d < t < 1500 \, d)$ with $R_1 = 0.07$ and $R_2 = 0.67$. At this point (day 1500), the light was changed to dim LL and the SCN remained in the partially synchronized two-cluster state. The previously applied light protocol thus creates initial conditions that can steer the system to the corresponding final state. This is indicative of hysteresis, i.e., different behaviors can be obtained at the same light intensity with increasing or decreasing light intensities. In other words, the very same SCN can exhibit split or non-split circadian state depending on the light protocol that was applied before dim LL because of the bistability.

C. Phase model description of cluster stability in the SCN model

The numerical simulations imply that the phase synchronization in the SCN occurs with stable one-cluster states

in DD and dim LL and with stable two-cluster states in dim and bright LL conditions. To confirm that these states occur due to synchronization with the interactions of the phases of oscillations, we derived phase model for the globally coupled SCN system and analyzed the stability of the one- and two-cluster states as a function of light intensity *L*. A generalized Kuramoto-type phase model⁶³ was considered,

$$\frac{\mathrm{d}\theta_k}{\mathrm{d}t} = \omega_k + \sum_{j=1}^N H(\Delta\theta_{k,j}),\tag{10}$$

where ω_k is the natural frequency of the k oscillator and $\Delta\theta_{k,j}$ = $\theta_j - \theta_k$ is the phase difference. $H(\Delta\theta_{k,j})$ is the interaction function between oscillators k and j. The phase shift due to some coupling can be obtained from the infinitesimal phase response curve $(Z(\theta))$ and from the perturbation $(s_{k,j})$ experienced by node k as a result of being coupled to node j as $d\theta_k = Z(\theta_k)s_{k,j}$ dt. Because in our example, the coupling is through parameter $v_{s,k}$, the overall perturbation with coupling strength α and $K_I = 1$ nM is

$$s_{k,j}(M_j, M_k, P_{\text{nuc},k}) = \alpha (M_j - M_k) \frac{1}{1 + P_{\text{nuc},k}^4}.$$
 (11)

Then, the interaction function H can be expressed as function of phase difference with averaging the phase shift for a cycle length for the two oscillators with a given (fixed) phase difference, i.e.,

$$H(\Delta\theta) = \frac{1}{2\pi} \int_{\theta=0}^{2\pi} Z(\theta) s \left[M(\theta + \Delta\theta), M(\theta), P_{\text{nuc}}(\theta) \right] d\theta \qquad (12)$$

The stability of the cluster synchronization states can be analytically calculated for a globally coupled population of identical oscillators (with the same natural frequency, waveform, response function for each oscillators, and thus identical *H*).⁶⁹ The stability of the one-cluster state can be expressed using the slope of the

09 August 2023 16:17:27

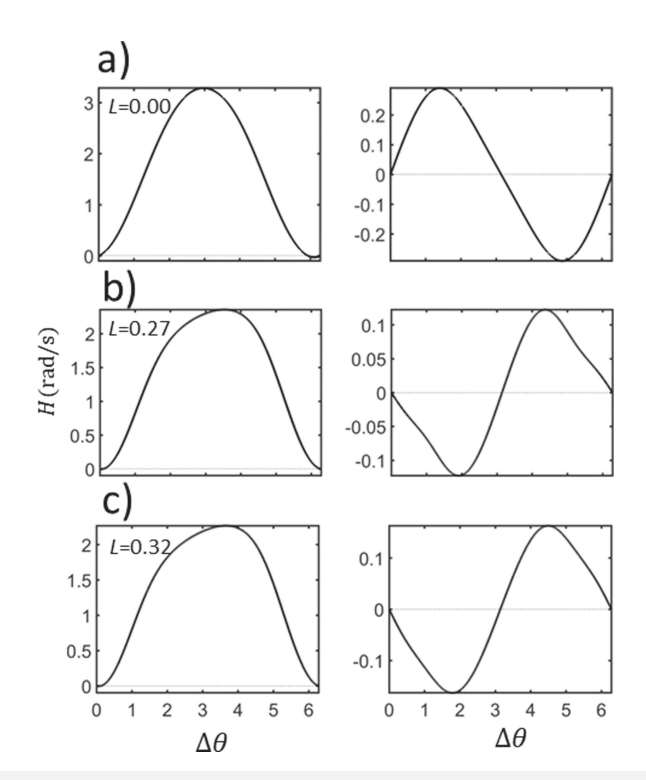


FIG. 5. Circadian phase interaction functions calculated with the phase sensitivity function method for a phase model of the simulated SCN. Left column: *H*. Right column: Odd part of *H*. (a) DD. (b) Dim LL. (c). Bright LL.

interaction function at $\Delta\theta = 0$,

$$\lambda_1 = \Gamma'(0), \tag{13}$$

where $\Gamma(\Delta\theta) = H(-\Delta\theta)$. When $\lambda_1 > 0$ or < 0, the one-cluster state is unstable or stable, respectively.

There could be many two-cluster states with different number of elements in each cluster, pN and p(1-N), where p is the cluster partition coefficient. The stability can be expressed with three distinct nontrivial eigenvalues, ⁶⁹

$$\lambda_1 = p\Gamma'(0) + (1 - p)\Gamma'(\Delta\theta),\tag{14}$$

$$\lambda_2 = (1 - p)\Gamma'(0) + p\Gamma'(-\Delta\theta),\tag{15}$$

$$\lambda_3 = (1 - p)\Gamma'(\Delta\theta) + p\Gamma'(-\Delta\theta),\tag{16}$$

where $\Delta\theta$ is the phase difference between such clusters. Because the numerically observed cluster states are quite balanced (about the same number of elements in each cluster), we consider p=0.5, where the phase difference between the clusters is π . The stability of the two-cluster state can be obtained by examining the real part of the largest eigenvalue, with $\text{Re}(\lambda_{\text{max}})>0$ for an unstable and <0 for a stable state.

The advantage of the phase model representation of the SCN is that as soon as H is obtained, we can analytically calculate the stability of the clusters. Then, the stability of the clusters can

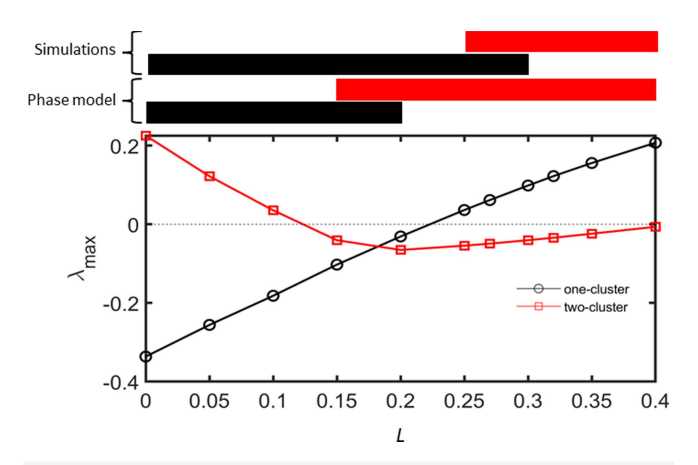


FIG. 6. Theoretical characterization of the stability of one- and two-cluster states in the single population SCN using the largest eigenvalues from phase-sensitivy based circadian interaction functions and comparisons to direct numerical simulations of the ODE model. $\lambda_{\rm max}$ as a function of the light intensity for the one- and two-cluster states using interaction functions obtained from phase sensitivity functions. $\lambda_{\rm max} < {\rm or} > 0$ indicate stable or unstable clusters, respectively. The eigenvalues were analytically calculated from H using Eq. (13) for the one-cluster and Eqs. (14)–(16) for the two-cluster state. On top, the black (one-cluster) and red (two-cluster) bars represent the stable cluster predicted by the phase model and corresponding numerical simulations, as indicated.

be obtained for a large range of light intensity without extensive numerical simulations. We used the XPPAUT software package 70 to calculate H.

D. Interaction function to predict cluster stability in the SCN model

Figure 5 shows the circadian phase interaction functions and their odd part at different light intensities. Only the odd components contribute to the stability for the considered clusters because the eigenvalues in Eqs. (13)–(16) depend on the derivatives of Γ (and thus H) at $\Delta\theta=0$ and π . The even parts of H do not contribute to the stability of the clusters but do impact the frequency of the synchronized oscillations.⁶⁹

Figure 5(a) shows H and the odd part for DD conditions. Under these conditions, the odd part is nearly a sinusoidal signal, but the overall H has large cosine component and thus H>0 for almost any phase difference. The slope of the odd part of H at zero is positive, and thus the one-cluster state is stable ($\lambda_1=-0.33<0$). For the two-cluster state $\lambda_{\rm max}=0.22>0$ and thus the phase model predicts the two-cluster state to be unstable. These predictions agree well with the direct numerical simulations of the SCN that showed a tightly synchronized one-cluster state. Under these DD conditions, where the circadian cells are close to a supercritical Hopf bifurcation, 49 the dominant components of the interaction function are $[1-\cos(\Delta\theta)]$ and $\sin(\Delta\theta)$, which agree well Kuramoto's theoretical prediction. 51

Figure 5(b) shows H and the odd part in dim LL conditions. While the overall shape of H looks similar to that in DD [Fig. 5(a)] with a shift of the maximum to a larger phase difference, a close

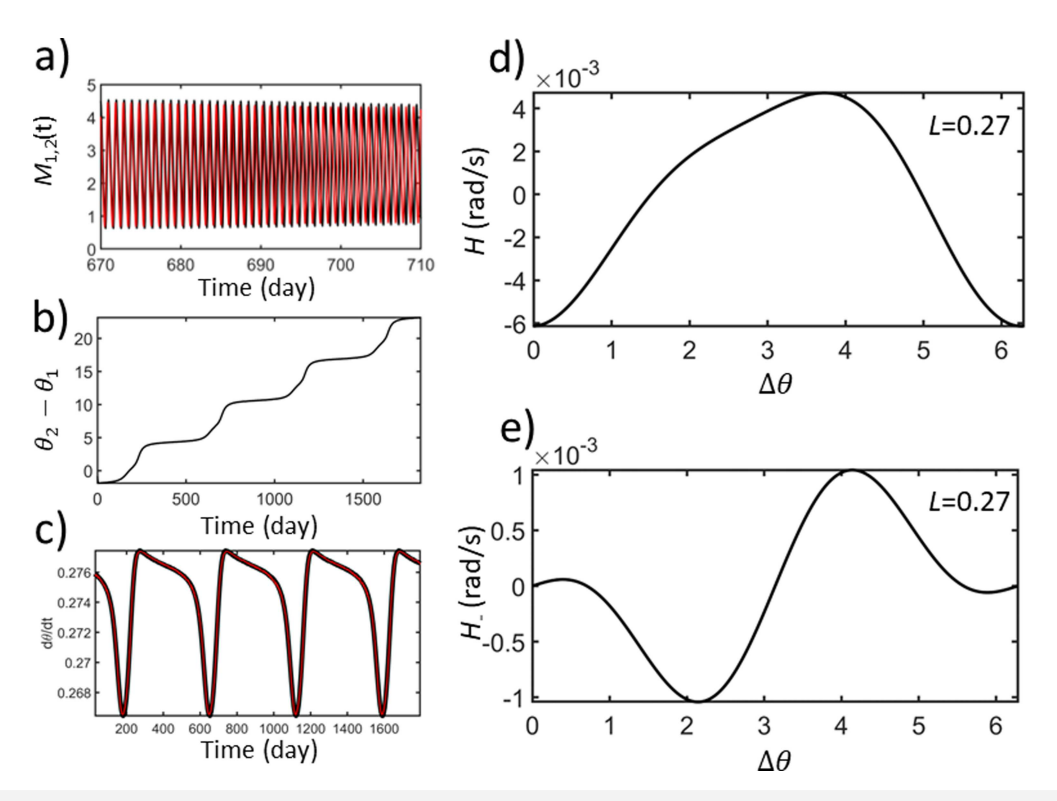


FIG. 7. Numerical simulations with two coupled circadian cells in dim LL for extracting data-based phase interaction functions (H). The numerical simulations were performed with two coupled cells ($\tau_1 = 1.0026$, $\tau_2 = 0.9974$, $\alpha = 0.018$). (a) Time series of $M_k(t)$ at dim LL (L = 0.27). (b) Phase difference as a function of time. (c) Instantaneous frequencies vs. time for oscillator 1 (black line: numerical simulations, red line: phase model fit). (d) H vs $\Delta\theta$. (e) Odd part of H.

inspection of the shape reveals that the odd part now is close to a — sin function, and thus the negative slope of H(0) indicates an unstable one-cluster state ($\lambda_1=0.06>0$). However, the odd part also shows the presence of higher harmonics ($\sin(2\Delta\theta)$), and overall the two-cluster state becomes stable with $\operatorname{Re}(\lambda_{\max})=-0.05<0$. In comparison with the direct numerical simulations, the phase model incorrectly predicts that the one-cluster state is unstable, and correctly predicts that the two-cluster state is stable. Figure 5(c) shows H and the odd part in bright LL conditions—in this case the interaction function is similar to the dim light case [Fig. 5(b)]—and thus phase model correctly predicts unstable one- and stable two-cluster states with $\lambda_1=0.12>0$ and $\operatorname{Re}(\lambda_{\max})=-0.03<0$.

To further explore the accuracy of phase model predictions of cluster stability in the single population SCN, we reconstructed the interaction functions at several light intensities. The largest eigenvalues for the one- and the two-cluster states as functions of light intensity are shown in Fig. 6. At low light intensities, from L=0.00 to L=0.10, where the oscillatory behavior of the cells was smooth, the one-cluster state was stable ($\lambda_{\rm max}<0$). When the light intensity increases (L=0.15 to L=0.20), the circadian phase interaction function changes, and now both the one- and two-cluster states are stable. At these light intensities, the phase model predicts bistability. Subsequently, with increased light from L=0.25 to L=0.40, the one- and two-cluster state were found to be unstable and stable, respectively.

For comparison, we performed direct numerical simulations at the different light intensities, and at the top of Fig. 6, the predicted stability of the one- and the two-cluster states are shown. The interval of the one-cluster state was found to be larger compared to the phase model predictions. Conversely, the simulations yielded a narrower range of the two-cluster state than that predicted by the phase models. The bistability in the simulations was observed at L=0.25 to L=0.30 at larger light intensities than those predicted by the phase model.

Overall, the phase model and the simulations follow the same trend. At low light intensity, the one-cluster is stable. At intermediate light intensity, the system showed bistability between the one-and two-cluster states. At larger values of L, only the two-cluster state was stable. However, there is some discrepancy in the predicted ranges; this discrepancy could be due to the cell heterogeneities used in the simulations, nonlinearity effects on the waveform and the phase response function, and strong coupling effects.

E. Cluster state predictions with data-based phase model

An alternative way to obtain phase models for coupled oscillators is with the use of a data-based approach when the instantaneous frequencies of the oscillators are recorded at a given coupling strength, and a phase model is fitted to the data to Eq. (10).⁵⁵ Then,

once H is obtained, predictions can be made using the phase model at different coupling strength, topology, and natural frequencies. Here, we test the use of the data-based technique to improve the predictions of the stability of the one- and the two-cluster states in the SCN.

The $M_k(t)$ time series of two weakly coupled ($\alpha=0.018$) circadian clock cells ($\tau_1=1.0026$ and $\tau_2=0.9974$) at L=0.27 are shown in Fig. 7(a). With these coupling strengths, the system exhibits a partially synchronized state, where the oscillators alternate between synchronized and desynchronized intervals. Correspondingly, the phase difference vs time plot [Fig. 7(b)] shows alternation of flat (phase synchronized) and quickly increasing (desynchronized) periods—such state is often called phase slipping dynamics. The instantaneous frequency of oscillator 1 as a function of time is shown Fig. 7(c). A periodic variation can be observed on a time scale of about 474 days. During the synchronized intervals, the frequency is nearly constant, and during the desynchronization interval, there is a large drop and subsequent increase in the frequency. Rearranging the phase model equation

$$\frac{\mathrm{d}\theta_1}{\mathrm{d}t} = \omega_1 + H(\Delta\theta),\tag{17}$$

$$\frac{\mathrm{d}\theta_1}{\mathrm{d}t} - \omega_1 = H(\Delta\theta),\tag{18}$$

the interaction function can be obtained by plotting $d\theta_1/dt - \omega_1$ as a function of the phase difference $\Delta\theta = \theta_2 - \theta_1$ and fitting the function with a truncated Fourier series. Truncating the interaction function up two Fourier terms is sufficient; the instantaneous frequencies obtained from the reconstructed phase model (red line) can nearly perfectly recover the numerically obtained values (black line) in the instantaneous frequency variations in Fig. 7(c).

The obtained H and its odd part are shown in Figs. 7(d) and 7(e). Compared to the phase sensitivity function based interaction functions [Fig. 5(b)], H and the odd part exhibit stronger higher harmonics. In particular, the slope of the odd part [see Fig. 7(e)] at zero phase difference is now positive, and thus the one-cluster state is stable ($\lambda_1 = -2.2 \times 10^{-4} < 0$). Similarly, strong second harmonics dominate the shape, and the two-cluster state is also stable ($\lambda_{\rm max} = -9.5 \times 10^{-4} < 0$). Therefore, the data-based phase model now correctly predicted the bistability between one- and two-cluster state in dim LL conditions.

The interaction function using the data-based technique was obtained for a range of light intensities ($0 \le L \le 0.4$), and the stability of the one- and the two-cluster states is shown as a function of L in Fig. 8. Similar to the phase model predictions using the phase response curve method, at low light intensities, only the one-cluster is stable ($0 \le L \le 0.1$). At intermediate light intensities, there is bistability between the one-and the two-cluster states ($0.15 \le L \le 0.27$). At large light intensity ($0.3 \le L \le 0.4$), the two-cluster state is stable. The data-based phase model approach now better predicts the stability compared to the numerical simulations (see the top of Fig. 8) but still predicts somewhat lower critical light intensity for the upper bound ($L_{\rm crit} = 0.27$ vs 0.30) of the stable one-cluster state and somewhat lower critical light intensity ($L_{\rm crit} = 0.15$ vs 0.25) for the lower bound of the stable two-cluster state.

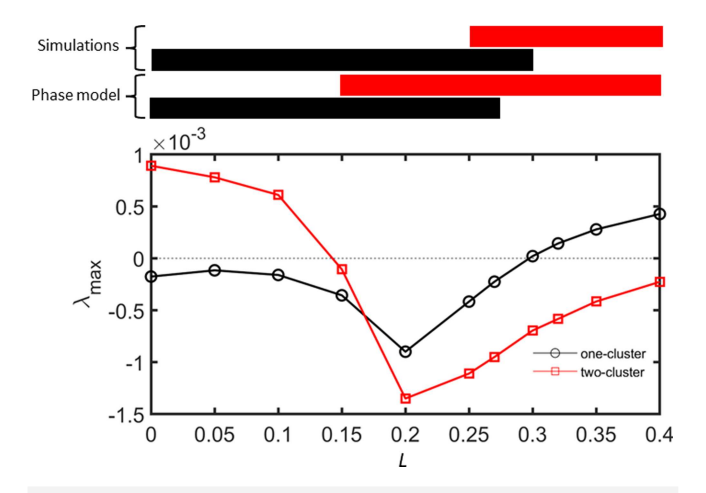


FIG. 8. Theoretical characterization of the stability of one- and two-cluster states in the single population SCN using the largest eigenvalues from data-based phase interaction functions and comparisons to direct numerical simulations of the ODE model. λ_{max} as a function of the light intensity for the one- and two-cluster states using data-based interaction functions. $\lambda_{\text{max}} < \text{or} > 0$ indicate stable or unstable clusters, respectively. The eigenvalues were analytically calculated from H (obtained simulations similar to those in Fig. 7 for each L) and using Eq. (13) for the one-cluster, and Eqs. (14)–(16) for the two-cluster state. On top, the black (one-cluster) and red (two-cluster) bars represent the stable cluster predicted by the phase model and corresponding numerical simulations, as indicated.

F. Cluster formation and chimera state in a modular SCN network

The bistability between the one- and the two-cluster states in dim LL opens the possibility for the existence of weak-chimera states in a modular network. One of the simplest of such networks can be constructed with two globally coupled population with weak cross coupling.²² For a weak-chimera state to exist in the circadian clock, the one- and two-cluster states must have different synchronization frequencies. This requirement implies a sufficient amount of nonisochronicity, (or phase shear) in the interaction function due to a large cosine component in $H^{22,25}$ As shown in the reconstructed interaction functions (in Figs. 5 and 7) the interaction functions do have large cosine components. Because H(0) is close to zero, in the (fully synchronized) one-cluster state, the synchronized frequency of the SCN is close to mean of the natural frequencies. However, in the two-cluster state, because $H(\phi) > 0$, the anti-phase synchronized oscillator pairs will have a tendency to have larger frequencies (and thus lower periods). In other words, the interaction speeds up the anti-phase synchronized clusters of the circadian clock. This was demonstrated in numerical simulations in Figs. 2(b) and 2(c), where the synchronized periods in dim LL conditions were 23.38 h and 22.55 h for the one- and the two-cluster states, respectively.

Motivated by the predictions of the phase models and simulations with a globally coupled network regarding cluster stability, we explored the behavior of a modular network consisting of two populations with a weak cross coupling. The two populations can represent two densely coupled circadian cells domains in the brain,

Chaos ARTICLE pubs.aip.org/aip/cha

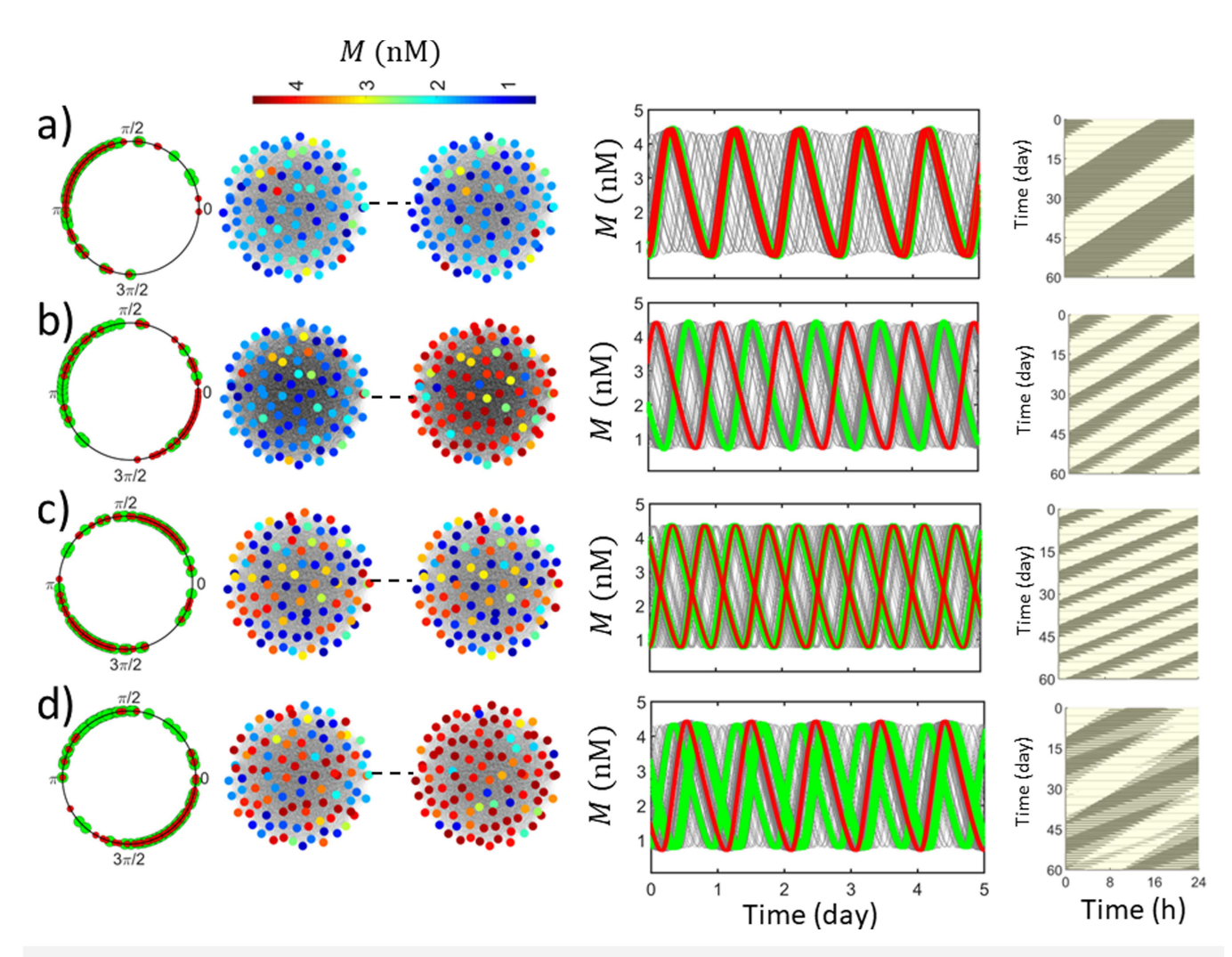


FIG. 9. Synchronization states of the SCN in dim LL using a modular network. From left to right: snapshot of phase, snapshot and time series of $M_k(t)$, and actogram. The modular network was constructed with $\alpha=2.10\times10^{-4}$ coupling strength in each populations with a weak cross coupling $\epsilon=0.15$. (a) Non-split state from one-cluster initials condition such that the two population are nearly in-phase. (b) Split circadian rhythm with one-cluster initial conditions that are anti-phase synchronized. The SCN yields spatial domains that are anti-phase to each other. (c) Split circadian rhythm with two-cluster initial conditions. The SCN yields two-cluster state without spatially localized in-phase synchronization. (d) Weak-chimera state with two-cluster initial condition for population 1, and one-cluster initial condition for population 2. The panels show the final synchronization states. Population 1: cells 1–100. Population 2: cells 101–200. In the time series plot in the third column, the green and red lines represent the synchronized elements in population 1 and 2, respectively, and the grey lines are the desynchronized elements. All simulations were performed with the same model parameters (L=0.26), only the initial conditions were different.

which are coupled relatively weakly to each other. For example, on a macroscopic scale, the two populations can represent the left and the right brain SCN in hamster. 40,41

N=100 cells were placed in each population, with relatively strong, all-to-all coupling in each population ($\alpha=2.10\times 10^{-4}$) and weak, all-to-all coupling between the populations ($\alpha\epsilon=3.15\times 10^{-5}$, i.e., $\epsilon=0.15$). The light intensity was fixed in dim LL (L=0.26), where there is bistability between the one- and the two-cluster states. (The light intensity was slightly decreased compared to the previous dim LL conditions so that the one- and

the two-cluster states are further away from their corresponding critical light intensities). The simulations were performed at exactly the same parameter values but with initial conditions corresponding nearly to one- or two-cluster states in each modules; the results are shown in Fig. 9 (phase snapshots, snapshot and time series plot of $M_k(t)$, and actograms) and Fig. 10 for phase differences.

When both SCN populations were started from nearly a onecluster state and the phase difference was small, the one-cluster populations synchronized in nearly in-phase conditions [see Figs. 9(a) and 10(a)]. This state thus represents a globally synchronized Chaos ARTICLE pubs.aip.org/aip/cha

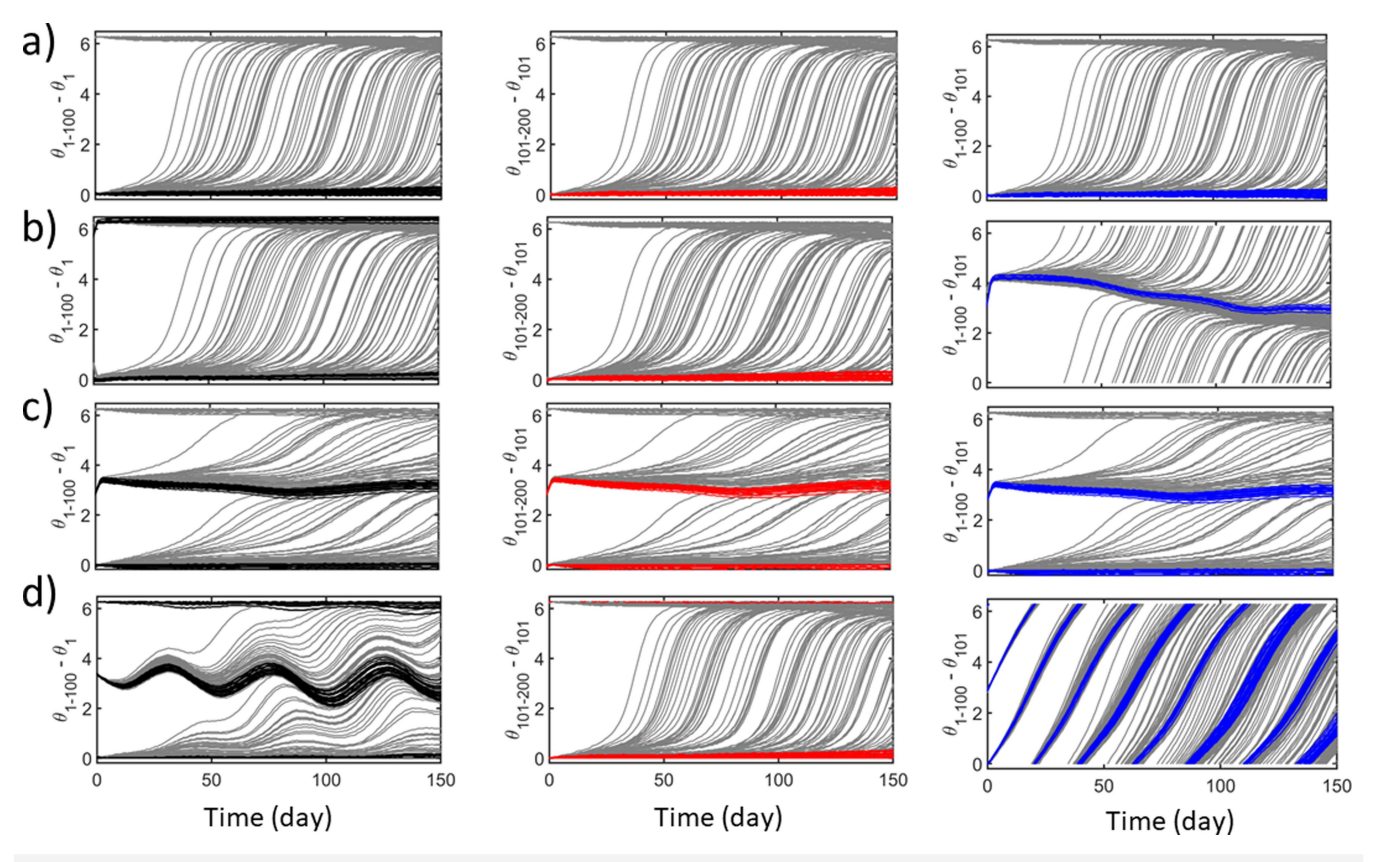


FIG. 10. Time series of phase differences among the circadian gene expression oscillations of the cells in the modular SCN network. The simulations of the circadian rhythms are at the same parameter values but differ by the initial conditions. The left column: phase differences in population 1 (black lines, $\theta_{1-100} - \theta_1$). Middle column: Phase differences in population 2 (red lines, ($\theta_{101-200} - \theta_{101}$). Right column: Phase differences between oscillators in the different populations (blue lines, $\theta_{101-200} - \theta_{101}$). Panels (a)–(d) correspond to those in Fig. 9. Population 1: cells 1–100. Population 2: cells 101–200. (a) One-cluster state in each populations, and in-phase synchronization between the populations. (b) One-cluster state in each populations, and synchronization between cells in different populations can be in- or anti-phase. (d) Chimera state: Two-cluster state in population 1, one-cluster state in population 2, and lack of synchrony in-between the populations. The black, red, and blue curves in the left, middle, and right panels, respectively, denote the behavior of the synchronized opening the panels, respectively.

one-cluster state, and thus there is no splitting in the circadian rhythm. The period of this synchronized state was 23.32 h.

When the one-cluster synchronized populations were started from a nearly anti-phase initial conditions relative to each other [see Figs. 9(b) and 10(b)], both populations remained in the one-cluster state; however, they reached an anti-phase synchronized state relatively to each other. This state represents a split circadian rhythm, where anti-phase synchronization was established between the two populations, but the one-cluster synchrony remained within each population. The period of this synchronized state was 23.16 h, i.e., the oscillators sped up compared to the globally synchronized one-cluster state (with period 23.32 h) as expected by the phase model analysis.

When the two populations were initialized in a nearly two-cluster initial state, both populations remained in the two-cluster state [see Fig. 9(c)] and two populations collectively synchronized in an "in-phase" configuration such that the phase differences between

pairs of elements in populations 1, in population 2, or between the populations are nearly zero or π [see Fig. 10(c)]. This state also represents a split circadian rhythm, however, now we do not see large domains of circadian cells with similar phases; instead, the cluster configuration depends on the initial conditions. We see a further decrease in the synchronized period, now to 22.80 h.

Finally, the observed synchronization pattern is shown in Figs. 9(d) and 10(d) when population 1 was started from a nearly two-cluster, and population 2 from a nearly one-cluster initial condition. Both populations remained in their corresponding states, i.e., population 1 synchronized with a two-cluster state and population 2 with a one-cluster state. However, in contrast to the previous examples, the two populations did not synhchronize with each other, as they attained 22.81 h (population 1) and 23.24 h (population 2) periods. The analysis of the phase differences [Fig. 9(d)] shows that within population 1, we can find in- and anti-phase synchronized pairs (left column); in population 2, the phase differences are close

09 August 2023 16:17:27

to 0 (or 2π), i.e., the population 2 is in a one-cluster synchronized state. The phase differences between elements in different populations diverges [right column in Fig. 10(d)]. We thus see that the SCN exhibits a weak-chimera synchronized state with desynchronization between the population. Note also that for the phase differences within population 1, the anti-phase state exhibits a slowly varying, oscillatory behavior, typically seen with weak chimeras as predicted by phase model theories and confirmed in experiments. 25,26 (To further confirm the simulation results, we repeated the simulations for random initial conditions as well as with identical oscillators; we identified only the above described dynamical states.) We thus see that a modular network of SCN cells can exhibit weak-chimera states. In this state, there is a domain with a one-cluster state, and another domain with two-cluster, split rhythm. In terms of actograms, we can discern three activity bands, one (wide) band corresponding to the one-cluster state (with its own period) and a double band (separated by about 12h) corresponding to the split population. (Note that when the bands overlap, the activity is larger, which is perceived as a darker shade in the actogram.)

IV. CONCLUSIONS

We investigated the synchronization patterns of globally coupled and modular networks of transcriptional oscillator models for circadian rhythms. With global coupling, numerical simulations and phase model predictions followed a similar trend: one-cluster state at low light intensity (L), bistability between one- and two-cluster states with intermediate L, and two-cluster states at high L. The phase models were constructed by both phase sensitivity function and data-based approaches. Analytical analysis of the stability of the cluster states predicted the lower bound of the two-cluster states lower than those observed in simulations. This is expected because the numerical simulation was performed with heterogeneous oscillators, but the phase model predictions assumed identical oscillators. Heterogeneities often (but not always⁷¹) have a tendency to destroy synchronization states and, thus, predictions with identical oscillators are expected to overestimate the stability regions compared to a heterogeneous population. In contrast, the upper bounds of the stability region of numerically observed one-cluster states were found to be larger than those predicted by both phase models, i.e., the ODE model with heterogeneous oscillators showed synchronization where the corresponding phase model with identical oscillators did not. This could be related to the deviation of the ODE model from strictly phase model behavior due to strong coupling and amplitude effects.

The two-cluster states arise because of higher (often second) harmonics in the phase interaction function due to nonlinearities in the oscillator properties. Similar to the transcriptional model considered here, the number of phase clusters increased as the oscillator properties were set further away from a Hopf bifurcation with the Brusselator, electrochemical oscillators, and an integrate-and-fire neuronal spiking model. Ta,74 In all these examples, many stable cluster states, including the one- and two-cluster states, co-existed at a given set of model parameters. It appears that there could be some commonality in the appearance of the nonlinearities in these models as a bifurcation parameter is changed, although there is no canonical, general oscillator model for behavior further away from Hopf

bifurcations; instead, the higher order contributions should be evaluated on a case-by-case basis. ⁷³ Nonetheless, when the light intensity would be further increased even larger number of clusters could be expected and eventually the system could become desynchronized. The previous SCN model⁴⁹ investigated such a large light intensity parameter region ($L \approx 1$), where weak coupling was not be able to synchronize the population.

Based on the assumption that light increased the maximum transcription rate, the model predicted that the very same coupling that synchronizes the oscillators to a one-cluster state in DD will induce a two-cluster state corresponding to a split circadian rhythm. The simulations revealed two fundamentally different types of split rhythm: with globally coupled single population, a stable two-cluster state can be obtained, where the clusters do not form discernible domains and the cluster configurations are determined by initial conditions. Such states were also observed with a modular coupling topology. However, with modular coupling, another type of split rhythm was also possible when each of the two populations is synchronized to a one-cluster state, but the collective rhythms of the two populations are anti-phase synchronized. This latter is consistent with the experimental observation that split circadian rhythm in hamsters is due to anti-phase synchronization of the left- and the right-brain SCN. 40,41 It should also be noted that with other animal models and different light protocols, the synchronization can form complex structures such as desynchronization,⁷⁵ ventral-dorsal (in contrast to left-right) anti-phase oscillations, 45,76 and asymmetries in addition to the left-right split.⁷⁷ In particular, the presence of two clocks in each side of the SCN⁴⁵ can be consistent with our computational predictions in dim LL where the two-cluster states in each module are synchronized.

In dim LL, the simulations predicted bistability between split and non-split circadian rhythm. This prediction can explain that when animal models are transferred to the LL condition, only about 50% shows the split circadian rhythm.³⁸ It is possible that the different animals have different extents of synchronization in DD due to animal-to-animal changes in the SCN properties, and thus only those animals with less synchronized initial conditions can produce splitting. Light pre-treatment procedures have been used in practical settings to improve the stability of splitting. 78,79 The simulations also point out a difficulty in studying the split rhythm as the transient times can be long (months or even years), which further complicate obtaining accurate dynamical information about the synchronization structures in the SCN. Nonetheless, the simulations predict that the applied light intensity plays an important role in the splitting behavior, and thus further experiments with varying light intensities are essential in improving the description of the spatiotemporal organization of the gene expressions in the SCN.

In dim LL conditions where in a single population there was a bistability between the one-cluster and two-cluster states, in a modular network the simulations predict a weak-chimera state where one population remains in one-cluster and the other in a two-cluster state with different frequencies (or periods). These states have similar dynamical properties to those predicted by phase models, numerical simulations, and experiments with electrochemical oscillators.^{25,26} In terms of actograms, such a state could be detected by three bouts of activity: one band for the one-cluster state with a given period and two bouts separated by 12 h with a different

period. Note that the detection of such rhythms in the experiment is complicated by various factors. First, long recording is required to separate overlapping activities, and second initial conditions are required where one population starts in one-cluster and the other population in the two-cluster states. In the experiments with electrochemical oscillators, 25,26 synchronization engineering techniques 16 were applied to design initial states with the closed loop feedback techniques. Optogenetic perturbation could provide a means to implement such feedback;80 however, concurrent imaging bioluminescent markers in the SCN slice is difficult because the isolated SCN lacks retinal input so that the cells remain synchronized to each other but not to environmental inputs.^{81,82} Long exposures to light conditions that induce splitting behavior could result in an adaptation of the circadian network rewiring, similar to photoperiodic adaptation to summer/winter light cycles,83 so that some of the properties of the circadian behavior could be retained.

Some of the inspiration of the interest in chimera states originated from unihemispheric sleep of birds and dolphins. A Our proposed model predicts a chimera mechanism driven by the dynamics of the circadian system. This is quite different from other scenarios in which the synchronization of spiking neurons is modulated by circadian rhythms, resulting in chimeras on the very short time scale (on the order of seconds). For example, a brain model with Hindmarsh–Rose neural oscillators under periodic circadian modulation of the injected current parameter showed differences in the alternations of sleep-promoting and wake-promoting regions between the hemispheres. In contrast, in our model, the circadian drive of the SCN is split, which can affect the spiking behavior of the hemispherical neurons. This comparison illustrates that combination of brain models on different time-scales could open new avenues for complex chimera states in the brain.

ACKNOWLEDGMENTS

This work was supported by NIH-NIGMS under Grant No. 1R01GM131403-01. I.Z.K. acknowledges support from National Science Foundation under Grant No. CHE-1900011. J.L.O.-E. acknowledges financial support from CONACYT. I.Z.K. expresses gratitude for the organizers and the participants of the International Workshop Chimera States: From Theory and Experiments to Technology and Living Systems conference in the Max Planck Institute for Physics of Complex Systems in 2022 for the fascinating talks/posters and the stimulating discussions about the chimera dynamics.

AUTHOR DECLARATIONS

Conflict of Interest

The authors have no conflicts to disclose.

Author Contributions

Jorge Luis Ocampo-Espindola: Conceptualization (equal); Investigation (equal); Visualization (equal); Writing – original draft (equal). K. L. Nikhil: Conceptualization (equal); Writing – review & editing (equal). Jr-Shin Li: Conceptualization (equal); Writing – review & editing (equal). Erik D. Herzog: Conceptualization

(equal); Writing – review & editing (equal). **István Z. Kiss:** Conceptualization (equal); Supervision (equal); Writing – review & editing (equal).

DATA AVAILABILITY

The data that support the findings of this study are available from the corresponding author upon reasonable request.

REFERENCES

- A. S. Pikovsky, M. G. Rosenblum, and J. Kurths, *Synchronization: A Universal Concept in Nonlinear Sciences* (Cambridge University Press, Cambridge, 2001).
 M. Marek and I. Stuchl, "Synchronization in two interacting oscillatory systems," Biophys. Chem. 3, 241–248 (1975).
- ³M. F. Crowley and R. J. Field, "Electrically coupled Belousov-Zhabotinskii oscillators. 1. Experiments and simulations," J. Phys. Chem. **90**, 1907–1915 (1986).
- ⁴M. F. Crowley and I. R. Epstein, "Experimental and theoretical studies of a coupled chemical oscillator: Phase death, multistability and in-phase and out-of-phase entrainment," J. Phys. Chem. 93, 2496–2502 (1989).
- ⁵H. Fujii and Y. Sawada, "Phase-difference locking of coupled oscillating chemical systems," J. Chem. Phys. **69**, 3830–3832 (1978).
- ⁶K. Nakajima and Y. Sawada, "Experimental studies on the weak coupling of oscillatory chemical reaction systems," J. Chem. Phys. **72**, 2231–2234 (1980).
- ⁷M. Toiya, V. K. Vanag, and I. R. Epstein, "Diffusively coupled chemical oscillators in a microfluidic assembly," Angew. Chem. Int. Ed. **47**, 7753–7755 (2008).
- ⁸M. Toiya, H. O. Gonzalez-Ochoa, V. K. Vanag, S. Fraden, and I. R. Epstein, "Synchronization of chemical micro-oscillators," J. Phys. Chem. Lett. **1**, 1241–1246 (2010).
- ⁹ A. F. Taylor, M. R. Tinsley, F. Wang, Z. Y. Huang, and K. Showalter, "Dynamical quorum sensing and synchronization in large populations of chemical oscillators," Science 323, 614–617 (2009).
- ¹⁰ A. F. Taylor, M. R. Tinsley, F. Wang, and K. Showalter, "Phase clusters in large populations of chemical oscillators," Angew. Chem. Int. Ed. 50, 10161–10164 (2011).
- ¹¹T. Okano and K. Miyakawa, "Feedback-controlled dynamics in a two-dimensional array of active elements," Phys. Rev. E **80**, 026215 (2009).
- ¹²V. K. Vanag and I. R. Epstein, "Pattern formation in a tunable medium: The Belousov-Zhabotinskii reaction in an aerosol of microemulsion," Phys. Rev. Lett. 87, 228301 (2001).
- ¹³M. Wickramasinghe and I. Z. Kiss, "Synchronization of electrochemical oscillators," in *Engineering of Chemical Complexity* (Wolrd Scientific, New Jersey, 2013), pp. 215–236
- pp. 215–236.

 ¹⁴I. Z. Kiss, Y. Zhai, and J. L. Hudson, "Emerging coherence in a population of chemical oscillators," Science **296**, 1676–1678 (2002).
- ¹⁵I. Z. Kiss, Y. M. Zhai, and J. L. Hudson, "Predicting mutual entrainment of oscillators with experiment-based phase models," Phys. Rev. Lett. **94**, 248301 (2005)
- ¹⁶I. Z. Kiss, C. G. Rusin, H. Kori, and J. L. Hudson, "Engineering complex dynamical structures: Sequential patterns and desynchronization," Science 316, 1886–1889 (2007).
- ¹⁷P. Uhlhaas and W. Singer, "Neural synchrony in brain disorders: Relevance for cognitive dysfunctions and pathophysiology," Neuron **52**, 155–168 (2006).
- ¹⁸M. J. Panaggio and D. M. Abrams, "Chimera states: Coexistence of coherence and incoherence in networks of coupled oscillators," Nonlinearity 28, R67–R87 (2015).
- ¹⁹O. E. Omel'Chenko, "The mathematics behind chimera states," Nonlinearity 31, R121_R164 (2018)
- ²⁰D. Battogtokh and Y. Kuramoto, "Coexistence of coherence and incoherence," Nonlinear Phenom. Complex Syst. 5, 380–385 (2002), available at http://www.j-npcs.org/abstracts/vol2002/v5no4/v5no4p380.html.
- ²¹D. M. Abrams and S. H. Strogatz, "Chimera states for coupled oscillators," Phys. Rev. Lett. 93, 174102 (2004).
- ²²P. Ashwin and O. Burylko, "Weak chimeras in minimal networks of coupled phase oscillators," Chaos **25**, 013106 (2015).

- ²³C. Bick and P. Ashwin, "Chaotic weak chimeras and their persistence in coupled populations of phase oscillators," Nonlinearity 29, 1468–1486 (2016).
 ²⁴M. Thoubaan and P. Ashwin, "Existence and stability of chimera states in a
- ²⁴M. Thoubaan and P. Ashwin, "Existence and stability of chimera states in a minimal system of phase oscillators," Chaos 28, 103121 (2018).
- ²⁵C. Bick, M. Sebek, and I. Z. Kiss, "Robust weak chimeras in oscillator networks with delayed linear and quadratic interactions," Phys. Rev. Lett. **119**, 168301 (2017)
- ²⁶J. L. Ocampo-Espindola, C. Bick, and I. Z. Kiss, "Weak chimeras in modular electrochemical oscillator networks," Front. Appl. Math. Stat. 5, 38 (2019).
- ²⁷ A. T. Winfree, *The Geometry of Biological Time* (Springer, 1980), Vol. 2.
- ²⁸D. C. Klein, R. Y. Moore, S. M. Reppert et al., Suprachiasmatic Nucleus: The Mind's Clock (Oxford University Press, USA, 1991).
- ²⁹M. C. Antle and R. Silver, "Orchestrating time: Arrangements of the brain circadian clock," Trends Neurosci. **28**, 145–151 (2005).
- ³⁰E. D. Herzog, "Neurons and networks in daily rhythms," Nat. Rev. Neurosci. 8, 790–802 (2007).
- ³¹ T. Pavlidis, Biological Oscillators: Their Mathematical Analysis (Academic Press, New York, 1973).
- ³²R. Kronauer, "A quantitative model for the effects of light on the amplitude and phase of the deep circadian pacemaker, based on human data," Sleep **90**, 306–309 (1990).
- ³³J.-C. Leloup, D. Gonze, and A. Goldbeter, "Limit cycle models for circadian rhythms based on transcriptional regulation in *Drosophila* and *Neurospora*," J. Biol. Rhythms **14**, 433–448 (1999).
- ³⁴D. B. Forger and C. S. Peskin, "A detailed predictive model of the mammalian circadian clock," Proc. Natl. Acad. Sci. U.S.A. **100**, 14806–14811 (2003).
- 35 J.-C. Leloup and A. Goldbeter, "Toward a detailed computational model for the mammalian circadian clock," Proc. Natl. Acad. Sci. U.S.A. 100, 7051–7056 (2003).
 36 D. K. Welsh, D. E. Logothetis, M. Meister, and S. M. Reppert, "Individual neurons dissociated from rat suprachiasmatic nucleus express independently phased circadian firing rhythms," Neuron 14, 697–706 (1995).
- ³⁷S. Yamaguchi, H. Isejima, T. Matsuo, R. Okura, K. Yagita, M. Kobayashi, and H. Okamura, "Synchronization of cellular clocks in the suprachiasmatic nucleus," Science **302**, 1408–1412 (2003).
- ³⁸C. S. Pittendrigh and S. Daan, "A functional analysis of circadian pacemakers in nocturnal rodents: V. Pacemaker structure: A clock for all seasons," J. Comp. Physiol. **106**, 333–355 (1976).
- ³⁹J. A. Evans, J. A. Elliott, and M. R. Gorman, "Dynamic interactions between coupled oscillators within the hamster circadian pacemaker," Behav. Neurosci. 124, 87–96 (2010).
- ⁴⁰H. O. De La, X. Iglesia, J. Meyer, A. Carpino, and W. J. Schwartz, "Antiphase oscillation of the left and right suprachiasmatic nuclei," Science **290**, 799–801 (2000).
- ⁴¹H. O. De La Iglesia, J. Meyer, and W. J. Schwartz, "Lateralization of circadian pacemaker output: Activation of left- and right-sided luteinizing hormone-releasing hormone neurons involves a neural rather than a humoral pathway," J. Neurosci. 23, 7412–7414 (2003).
- 42 S. Daan and C. Berde, "Two coupled oscillators: Simulations of the circadian pacemaker in mammalian activity rhythms," J. Theor. Biol. **70**, 297–313 (1978).
- ⁴³M. Kawato and R. Suzuki, "Two coupled neural oscillators as a model of the circadian pacemaker," J. Theor. Biol. **86**, 547–575 (1980).
- ⁴⁴G. A. Oda and W. O. Friesen, "A model for 'splitting' of running-wheel activity in hamsters," J. Biol. Rhythms 17, 76–88 (2002).
- ⁴⁵L. Yan, N. C. Foley, J. M. Bobula, L. J. Kriegsfeld, and R. Silver, "Two antiphase oscillations occur in each suprachiasmatic nucleus of behaviorally split hamsters," J. Neurosci. **25**, 9017–9026 (2005).
- ⁴⁶P. Indic, W. J. Schwartz, and D. Paydarfar, "Design principles for phase-splitting behaviour of coupled cellular oscillators: Clues from hamsters with 'split' circadian rhythms," J. R. Soc. Interface 5, 873–883 (2008).
- ⁴⁷D. Gonze, S. Bernard, C. Waltermann, A. Kramer, and H. Herzel, "Spontaneous synchronization of coupled circadian oscillators," Biophys. J. 89, 120–129 (2005).
 ⁴⁸T.-L. To, M. A. Henson, E. D. Herzog, and F. J. Doyle, "A molecular model for intercellular synchronization in the mammalian circadian clock," Biophys. J. 92, 3792–3803 (2007).

- ⁴⁹S. Schroder, E. D. Herzog, and I. Z. Kiss, "Transcription-based oscillator model for light-induced splitting as antiphase circadian gene expression in the suprachiasmatic nuclei." I Biol. Rhythms 27, 79–90 (2012)
- suprachiasmatic nuclei," J. Biol. Rhythms 27, 79–90 (2012).

 50 K. Okuda, "Variety and generality of clustering in globally coupled oscillators," Phys. D 63, 424–436 (1993).
- ⁵¹Y. Kuramoto, *Chemical Oscillations, Waves & Turbulence* (Springer, Berlin, 1984)
- ⁵²G. B. Ermentrout and N. Kopell, "Multiple pulse interactions and averaging in
- systems of coupled neural oscillators," J. Math. Biol. 29, 195–217 (1991).

 53 I. T. Tokuda, S. Jain, I. Z. Kiss, and J. L. Hudson, "Inferring phase equations from multivariate time series," Phys. Rev. Lett. 99, 064101 (2007).
- ⁵⁴I. T. Tokuda, M. Wickramasinghe, and I. Z. Kiss, "Detecting connectivity of small, dense oscillator networks from dynamical measurements based on a phase modeling approach," Phys. Lett. A 377, 1862–1867 (2013).
- ⁵⁵S. Wang, E. D. Herzog, I. Z. Kiss, W. J. Schwartz, G. Bloch, M. Sebek, D. Granados-Fuentes, L. Wang, and J.-S. Li, "Inferring dynamic topology for decoding spatiotemporal structures in complex heterogeneous networks," Proc. Natl. Acad. Sci. U.S.A. 115, 9300–9305 (2018).
- ⁵⁶B. Kralemann, L. Cimponeriu, M. Rosenblum, A. Pikovsky, and R. Mrowka, "Uncovering interaction of coupled oscillators from data," Phys. Rev. E **76**, 055201 (2007).
- ⁵⁷J. Miyazaki and S. Kinoshita, "Determination of a coupling function in multi-coupled oscillators," Phys. Rev. Lett. **96**, 194101 (2006).
- ⁵⁸D. Gonze and A. Goldbeter, "Circadian rhythms and molecular noise," Chaos **16**, 026110 (2006).
- ⁵⁹U. Albrecht, "Invited review: Regulation of mammalian circadian clock genes," J. Appl. Physiol. **92**, 1348–1355 (2002).
- ⁶⁰ E. Contreras, A. P. Nobleman, P. R. Robinson, and T. M. Schmidt, "Melanopsin phototransduction: Beyond canonical cascades," J. Exp. Biol. 224, jeb226522 (2021).
- ⁶¹A. P. Patton, M. H. Hastings, and N. J. Smyllie, "Cells and circuits of the suprachiasmatic nucleus and the control of circadian behaviour and sleep," in *Sleep and Clocks in Aging and Longevity*, edited by A. Jagota (Springer International Publishing, Cham, 2023), pp. 33–70.
- ⁶²G. Freeman, R. Krock, S. Aton, P. Thaben, and E. Herzog, "GABA networks destabilize genetic oscillations in the circadian pacemaker," Neuron **78**, 799–806 (2013).
- ⁶³H. Daido, "Generic scaling at the onset of macroscopic mutual entrainment in limit-cycle oscillators with uniform all-to-all coupling," Phys. Rev. Lett. 73, 760–763 (1994).
- ⁶⁴R. Refinetti, G. Cornélissen, and F. Halberg, "Procedures for numerical analysis of circadian rhythms," Biol. Rhythm Res. **38**, 275–325 (2007).
- ⁶⁵J. C. Dunlap, J. J. Loros, and P. J. DeCoursey, *Chronobiology: Biological Time-keeping* (Sinauer Associates, Sunderland, MA, 2004).
- ⁶⁶C. S. Pittendrigh and S. Daan, "A functional analysis of circadian pacemakers in nocturnal rodents: I. The stability and lability of spontaneous frequency," J. Comp. Physiol. **106**, 223–252 (1976).
- 67 P. C. Molyneux, M. K. Dahlgren, and M. E. Harrington, "Circadian entrainment aftereffects in suprachiasmatic nuclei and peripheral tissues in vitro," Brain Res. 1228, 127–134 (2008).
- ⁶⁸S. J. Aton, G. D. Block, H. Tei, S. Yamazaki, and E. D. Herzog, "Plasticity of circadian behavior and the suprachiasmatic nucleus following exposure to non-24-hour light cycles," J. Biol. Rhythms **19**, 198–207 (2004).
- ⁶⁹ K. Okuda, "Variety and generality of clustering in globally coupled oscillators," Phys. D **63**, 424–436 (1993).
- ⁷⁰B. Ermentrout, Simulating, Analyzing, and Animating Dynamical Systems: A Guide to XPPAUT for Researchers and Students, Software, Environments, Tools (Society for Industrial and Applied Mathematics, Philadelphia, PA, 2002).
- ⁷¹ Y. Zhang, J. L. Ocampo-Espindola, I. Z. Kiss, and A. E. Motter, "Random heterogeneity outperforms design in network synchronization," Proc. Natl. Acad. Sci. U.S.A. 118, e2024299118 (2021).
- ⁷²S. Shirasaka, W. Kurebayashi, and H. Nakao, "Phase-amplitude reduction of transient dynamics far from attractors for limit-cycling systems," Chaos 27, 023119 (2017).

- ⁷³ H. Kori, Y. Kuramoto, S. Jain, I. Z. Kiss, and J. L. Hudson, "Clustering in globally coupled oscillators near a Hopf bifurcation: Theory and experiments," Phys. Rev. E 89, 062906 (2014).
- ⁷⁴H. Kori, I. Z. Kiss, S. Jain, and J. L. Hudson, "Partial synchronization of relaxation oscillators with repulsive coupling in autocatalytic integrate-and-fire model and electrochemical experiments," Chaos 28, 045111 (2018).
- ⁷⁵H. Ohta, S. Yamazaki, and D. G. McMahon, "Constant light desynchronizes mammalian clock neurons," Nat. Neurosci. **8**, 267–269 (2005).
- ⁷⁶L. Yan, R. Silver, and M. Gorman, "Reorganization of suprachiasmatic nucleus networks under 24-h LDLD conditions," J. Biol. Rhythms 25, 19–27 (2010).
- ⁷⁷M. Tavakoli-Nezhad and W. J. Schwartz, "c-fos expression in the brains of behaviorally 'split' hamsters in constant light: Calling attention to a dorsolateral region of the suprachiasmatic nucleus and the medial division of the lateral habenula," J. Biol. Rhythms 20, 419–429 (2005).
- ⁷⁸J. A. Evans, J. A. Elliott, and M. R. Gorman, "Dim nighttime illumination interacts with parametric effects of bright light to increase the stability of circadian rhythm bifurcation in hamsters," Chronobiol. Int. **28**, 488–496 (2011).
- ⁷⁹T. Noguchi, E. M. Harrison, J. Sun, D. May, A. Ng, D. K. Welsh, and M. R. Gorman, "Circadian rhythm bifurcation induces flexible phase resetting by reducing circadian amplitude," Eur. J. Neurosci. 51, 2329–2342 (2020).

- ⁸⁰J. P. Newman, M.-F. Fong, D. C. Millard, C. J. Whitmire, G. B. Stanley, and S. M. Potter, "Optogenetic feedback control of neural activity," eLife 4, e07192 (2015).
 ⁸¹C. Mazuski, S. P. Chen, and E. D. Herzog, "Different roles for VIP neurons in the neonatal and adult suprachiasmatic nucleus," J. Biol. Rhythms 35, 465–475 (2020)
- ⁸²M. H. Hastings, E. S. Maywood, and M. Brancaccio, "The mammalian circadian timing system and the suprachiasmatic nucleus as its pacemaker," Biology **8**, 13 (2019).
- ⁸³M. C. Tackenberg and D. G. McMahon, "Photoperiodic programming of the SCN and its role in photoperiodic output," Neural Plast. **2018**, 8217345 (2018).
- ⁸⁴N. Rattenborg, C. Amlaner, and S. Lima, "Behavioral, neurophysiological and evolutionary perspectives on unihemispheric sleep," Neurosci. Biobehav. Rev. **24**, 817–842 (2000).
- ⁸⁵T. A. Glaze and S. Bahar, "Neural synchronization, chimera states and sleep asymmetry," Front. Netw. Physiol. 1, 734332 (2021).
- ⁸⁶Z. Wang and Z. Liu, "A brief review of chimera state in empirical brain networks," Front. Physiol. 11, 724 (2020).
- ⁸⁷L. Ramlow, J. Sawicki, A. Zakharova, J. Hlinka, J. C. Claussen, and E. Schöll, "Partial synchronization in empirical brain networks as a model for unihemispheric sleep," Europhys. Lett. 126, 50007 (2019).